Electrocatalytic Activity of the Ni$_{57.3}$Co$_{42.7}$ Alloy for the Hydrogen Evolution

Zoran Grubač,* Antonija Sesar

Department of General and Inorganic Chemistry, Faculty of Chemistry and Technology, University of Split, Ruđera Boškovića 35, HR-21000 Split, Croatia
* Corresponding author's e-mail address: grubac@ktf-split.hr

—————— THIS PAPER IS DEDICATED TO PROF. MIRJANA METIKOŠ-HUKOVIĆ ON THE OCCASION OF HER BIRTHDAY ——————

Abstract: The hydrogen evolution reaction (HER) on Ni$_{57.3}$Co$_{42.7}$ alloy and its main components, polycrystalline nickel and cobalt was investigated in 1.0 mol L^{-1} NaOH solution at 20 °C using cyclic voltammetry, pseudo-steady-state linear polarization and electrochemical impedance spectroscopy methods. The purpose of investigation was to evaluate the effect of cobalt on the intrinsic catalytic activity of nickel. Cyclic voltammetry measurements, performed in a wide potential range from hydrogen to oxygen evolution, clearly showed the potential range of formation and reduction metal oxides / hydroxides. Electrocatalytic activity of the investigated electrodes was derived from pseudo-steady-state linear polarization curves, Tafel plots and electrochemical impedance spectroscopy (EIS). Electrochemical impedance spectra obtained in potential range of hydrogen evolution were modeled with modified Randles electric equivalent circuit. Kinetic parameters (the exchange current density and the cathodic Tafel slope), determined from linear polarization measurements and electrochemical impedance measurements, were compared for all three electrode materials. Ni$_{57.3}$Co$_{42.7}$ catalyst has shown better electrocatalytic activity compared with pure Co. The main pathway for the HER at investigated electrode materials is Volmer-Heyrovski with Heyrovsky as the rate determining step.

Keywords: hydrogen evolution, electrocatalysis, Ni-Co alloys, Ni, Co.

INTRODUCTION

IN industrial electrolysers the hydrogen evolution reaction (HER) is one of the most frequently involved electrochemical reaction, either as a desired reaction in the case of water electrolysis, or as a by-reaction in electroplating process.[1] The electrolysis of water, even if quite expensive due to its high energy consumption, is an important technique for hydrogen production.

The main electrode properties to be considered for water electrolysis are the large active surface area, good electrochemical stability and electrocatalytic activity, the low hydrogen overpotential, and high corrosion resistance.[2] It is known that Pt and other noble metals are identified as the most effective electrocatalysts for HER due to their low reduction overpotentials and fast reduction rate. Because of their high cost and low abundance, noble metals are not suitable for industrial production. Therefore high catalytic activity and stability, and a low cost make Ni and its alloys the most important electrode materials for the HER in alkaline solutions.
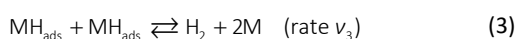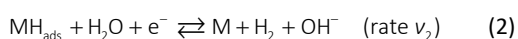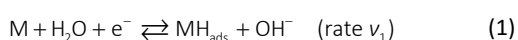
It is known that the catalytic activity of bare Ni towards the hydrogen evolution can be enhanced either by increasing the surface area or by alloying Ni mostly with transition metals in order to obtain electrodes with optimized adsorption characteristics. The electrocatalytic activity depends on the heat of adsorption of the intermediate on the electrode surface, in a way giving arise to the well-known 'vulcano' curve. A combination of two metals from the two brunches of vulcano curve could results in enhanced activity.[3]

The intrinsic activity of Ni has been improved by alloying Ni with metals such as Co, Fe, Mo, and W. It has been demonstrated that the alloying Ni with Co, in composition range between 41 and 64 weight percent, can improve the intrinsic catalytic activity of Ni as a consequence of the synergism among the catalytic properties of nickel (low hydrogen overpotential) and of cobalt (high hydrogen adsorption. [4,5,6 and references therein]

The hydrogen evolution reaction was intensively studied by the electrochemistry group of Professor Mirjana Metikoš Huković. The electrode material studied were polycrystalline[7,8] and nanocrystalline Ni,[7,9] sputter deposited Ni-W films,[9] electrodeposited Ni-15Mo alloy,[1,10] amorphous Zr-Ni alloys[11] and Co-Zr alloys.[12] The influence of alloying element, as well as the surface structure on the catalytic activity was investigated in these papers.

It is well established that the hydrogen evolution reaction on a metallic electrode, M, in alkaline solutions proceeds through the three step reaction mechanism with the only one type of intermediate. These steps are:

$$M + H_2O + e^- \rightleftharpoons MH_{ads} + OH^- \quad (\text{rate } v_1) \tag{1}$$

$$MH_{ads} + H_2O + e^- \rightleftharpoons M + H_2 + OH^- \quad (\text{rate } v_2) \tag{2}$$

$$MH_{ads} + MH_{ads} \rightleftharpoons H_2 + 2M \quad (\text{rate } v_3) \tag{3}$$

where the MH_{ads} represents the hydrogen adsorbed on the electrode surface. Steps (2) and (3) can take place simultaneously or interchangeably. The HER starts with the proton discharge (Volmer reaction, [Eq. (1)]), and follows either by the electrodesorption step (Heyrovsky reaction, [Eq. (2)]), or the H recombination step (Tafel reaction, [Eq. (3)]). The rate controlling step can be accomplished in terms of Tafel slopes or by calculating the rate constants of the forward and backward reactions through simultaneous fitting of polarization and impedance data. According to the general model for the HER mechanism, if the Volmer reaction [Eq. (1)] is the rate determining step (rds), the resulting Tafel curve should yield a slope of 118 mV dec^{-1} at 20 °C. If the Heyrovsky reaction is the rate determining step [Eq. (2)], the measured Tafel slope would yield a value of about 40 mV dec^{-1}, or 30 mV dec^{-1} for the Tafel desorption step [Eq. (3)].[11,12,13]

In the present work the kinetic parameters for the hydrogen evolution on the Ni-Co alloy were assessed by pseudo-steady-state polarization curves and electrochemical impedance spectroscopy in 1.0 mol L^{-1} NaOH solution, at 20 °C. The results were compared with results for catalytic activity of pure polycrystalline Ni and Co obtained under the same experimental conditions.

EXPERIMENTAL

Electrodes made from polycrystalline 99.9 % Ni, 99.99 % cobalt (Johnson Matthey) and Ni$_{57.3}$Co$_{42.7}$ alloy were used to study the HER in a 1.0 mol L^{-1} NaOH solution at 20 °C. The chemical composition of electrode materials was confirmed with X-ray fluorescence analysis using Thermo Fisher Scientific Niton XL3t XRF Analyzer. Electrodes for electrochemical measurements were prepared from 5 mm diameter rods inserted through a close-fitting hole in a polytetrafluoroethylene (PTFE) holder so that only the circular cross section was exposed to the electrolyte. Prior to the electrochemical measurements, the exposed face of polycrystalline electrode was first mechanically polished with 1200 grit emery paper followed by polishing with Buehler 1.0 µm, 0.3 µm and 0.05 µm Al$_2$O$_3$ powder. The final cleaning of the electrode was performed with ethanol in an ultrasonic bath.

All experiments were carried out in a standard three electrode cell. The counter electrode was a large area platinum electrode and the reference electrode, to which all potentials in the paper are referred, was an Ag / AgCl / saturated KCl (199 mV vs. standard hydrogen electrode, SHE). Before each measurement the oxide film formed on the electrode surface was reduced by potentiostatic polarization at −1.31 V for 60 s.

Cyclic voltammograms were recorded by sweeping the electrode potential from −1.5 V in anodic direction to various anodic limits and reversed to −1.5 V with a sweep rate v = 10 mV s^{-1}.

EIS measurements were performed at specified constant dc potentials in the frequency range from 60 kHz to 50 mHz using a Solartron Frequency Response Analyzer SI 1255 and Solartron Electrochemical Interface 1287 controlled by a PC. The experimental data were fitted using the complex nonlinear least squares (CNLS) fit analysis software ZView, and values of the elements of the proposed equivalent electric circuit were derived.
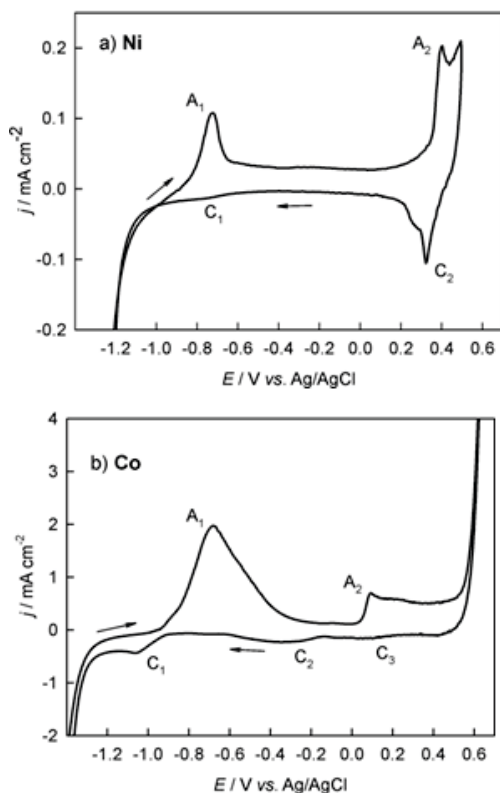
RESULTS AND DISCUSSION

Cyclic Voltammetry

Cyclic voltammetry measurements were performed in the potential range from hydrogen to oxygen evolution in order to examine the general behavior of the Ni, Co and Ni$_{57.3}$Co$_{42.7}$ electrodes in 1.0 mol L^{-1} NaOH solution. Measurements inside the potential range from the rest potential to the potential of hydrogen evolution were performed in order to gain the main kinetic parameters for the reaction of hydrogen evolution.

Cyclic voltammograms obtained for pure Ni and Co are shown in Figure 1a and Figure 1b, respectively. Electrochemical behavior of Ni electrode in an alkaline solution is in detail described in our previous work.[14] Briefly, an anodic current peak A$_1$ corresponds to both the Ni | α-Ni(OH)$_2$ transition and hydrogen oxidation. An abrupt increase in the anodic current density at higher anodic potentials and appearance of the current peak A$_2$ are due to the formation of a higher valent nickel oxide, the

NiOOH-type species. Its formation causes a slight decrease in the current density and the appearance of the secondary passivation of Ni. In a reverse potential sweep, the current peak C_2 corresponds to reduction of NiOOH to β-Ni(OH)$_2$. The current peak C_1 corresponding to α-Ni(OH)$_2$ reduction is followed by a current increase due to hydrogen adsorption and evolution.
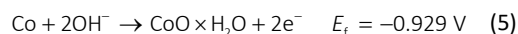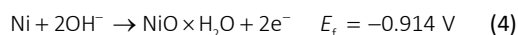
In cyclic voltammogram of Co two anodic and three cathodic current peaks are observed. The first anodic peak A_1 can be attributed to the oxidation of Co to Co(II) oxide / hydroxide (CoO / Co(OH)$_2$).[15] The growth of the Co(II) oxide / hydroxide layer passivates the surface and the current decreases. At potentials above 0.145 V, where the oxidation of Co(II) to either Co$_3$O$_4$ or CoOOH is thermodynamically allowed, the current increases again. The current peak A_2 is attributed to the conversion of CoO / Co(OH)$_2$ to a mixed Co(II/III) oxide in the bulk solid phase. At higher potentials ($E > 0.4$ V) a sharp increase in current density is assigned to the conversion Co(II/III) oxide to a Co(III) oxide. In reversed scan the reduction peak C_3 is assigned to the reduction of Co(III) oxide to a Co(II/III) oxide. The reduction peak C_2 represents the reduction of Co(II/III) oxide to Co(II) oxide / hydroxide and peak C_3 to the reduction Co(III) oxide / hydroxide to Co(OH)$_2$.[15]
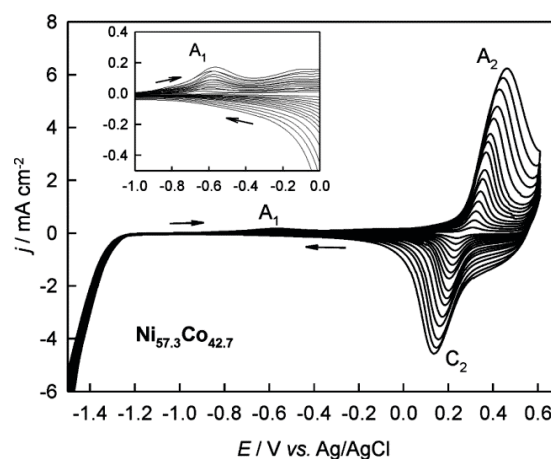
Cyclic voltammograms of Ni$_{57.3}$Co$_{42.7}$ alloy recorded with a progressively increasing sweep rates are presented in Figure 2. During the anodic sweep, the oxidation of the alloy surface starts at *ca.* −1.0 V and the current slowly increases up to −0.7 V forming a broad slightly expressed current peak A_1, after which the current plateau can be observed. At *ca.* −0.3 V the current starts to increase slowly making a shoulder up to ca. 0.15 V, after which a sharp increase in current and a current peak A_2 can be observed at *ca.* 0.30 V ($v = 10$ mV s^{-1}). Finally, at $E > 0.6$ V the reaction of oxygen evolution commences. The potential of the current peak A_2 shifts slightly towards positive potential values by increasing the sweep rate. On the cathodic portion of the voltammogram a well expressed cathodic current peak C_2 is observed at ca. 0.2 V ($v = 10$ mV s^{-1}). It slightly shifts towards negative potential values by increasing the sweep rate. The current increase at cathodic potentials more negative than *ca.* −1.2 V is caused by the hydrogen evolution.

It is known from literature that the anodic polarization curve of nickel[16–20] and cobalt[21–25] show the primary region of passivation in neutral and alkaline solutions by forming hydrated oxides in which metals are in the +2 oxidation state. The potentials E_f corresponding to their formation[26] at pH = 14 are:
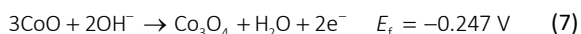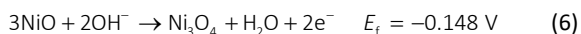
$$Ni + 2OH^- \rightarrow NiO \times H_2O + 2e^- \qquad E_f = -0.914 \text{ V} \qquad (4)$$

$$Co + 2OH^- \rightarrow CoO \times H_2O + 2e^- \qquad E_f = -0.929 \text{ V} \qquad (5)$$

Thus, the current peak A_1 of the Ni$_{57.3}$Co$_{42.7}$ alloy corresponds to the formation of both Co(OH)$_2$ and Ni(OH)$_2$.

Figure 1. The cyclic voltammograms for: a) Ni and b) Co recorded in 1.0 mol L^{-1} NaOH solution; $v = 10$ mV s^{-1}.
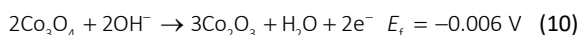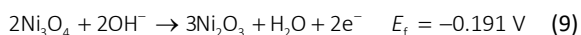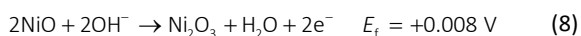

Figure 2. The cyclic voltammograms Ni$_{57.3}$Co$_{42.7}$ alloy recorded in 1.0 mol L^{-1} NaOH solution with progressively increasing sweep rates ($v = 10$–200 mV s^{-1}). Detail: Magnified area of the peak A_1.

The slight current increase at *ca.* −0.3 V can be connected with the further solid state oxidation of Ni(II) and Co(II) hydrated oxides present in the outer part of the oxide film according to the following reactions:[26]

$$3NiO + 2OH^- \rightarrow Ni_3O_4 + H_2O + 2e^- \quad E_f = -0.148 \text{ V} \quad (6)$$

$$3CoO + 2OH^- \rightarrow Co_3O_4 + H_2O + 2e^- \quad E_f = -0.247 \text{ V} \quad (7)$$

Finally, the current peak A_2 can be assigned to the formation of nickel and cobalt oxides with the +3 oxidation state[26] as follows:

$$2NiO + 2OH^- \rightarrow Ni_2O_3 + H_2O + 2e^- \quad E_f = +0.008 \text{ V} \quad (8)$$

$$2Ni_3O_4 + 2OH^- \rightarrow 3Ni_2O_3 + H_2O + 2e^- \quad E_f = -0.191 \text{ V} \quad (9)$$

$$2Co_3O_4 + 2OH^- \rightarrow 3Co_2O_3 + H_2O + 2e^- \quad E_f = -0.006 \text{ V} \quad (10)$$

As Co(III) oxide in the passivating film formed in alkaline solutions is not easily reduced,[21,24] it seems that the cathodic current peak C_2 corresponds dominantly to the cathodic reduction of Ni(III) to Ni(II) oxidation state. According to literature data[20] NiOOH and / or Ni_2O_3 can be easily reduced to NiO in alkaline solutions.

Figure 3 shows a series of cyclic voltammograms recorded with a $Ni_{57.3}Co_{42.7}$ alloy for several successive increases of the anodic sweep-reversal potential limit, E_{al}, from −0.65 V to 0.1 V. After oxidation of the alloy at potentials ranging from −0.9 to −0.5 V, the cathodic sweep shows a well pronounced current peak C_1 corresponding to the reduction of $Co(OH)_2$ and $Ni(OH)_2$. The peak potential
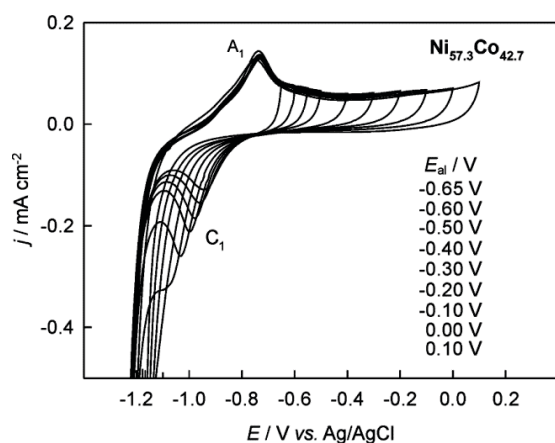
Figure 3. The cyclic voltammograms $Ni_{57.3}Co_{42.7}$ alloy recorded in 1.0 mol L^{-1} NaOH solution for a successive increase of the anodic potential limit from −0.65 V to 0.1 V; v = 10 mV s^{-1}.

C_1 significantly shifts towards catodic potential values when the anodic potential limit is more positive. This behavior is in accordance with those of pure metals; hydrated Co(II)[26] and Ni(II)[16–18] oxides formed during the early stage of anodic polarization undergo complete cathodic reduction to the zero oxidation state. For all cyclic voltammograms recorded up to the anodic potential limit of −0.5 V the values of charges corresponding to the current peaks A_1 and C_1 were almost equal. However, when the anodic potential limit increases above −0.5 V, the cathodic current peak C_1 disappears. The irreversibility in the formation and reduction of oxide films of Co and Ni with the +2 oxidation state, is linked to the stabilization of the Ni(II) hydroxide caused by its dehydration, *i.e.* its solid state transformation of $\alpha(Ni(OH)_2)$ to $\beta Ni(OH)_2$.[16,17,19] By increasing the anodic potential limit, the recorded cyclic voltammograms are almost identical to those presented in Figure 2.

## Electrocatalytic Activity for Hydrogen Evolution

The electrocatalytic activity of $Ni_{57.3}Co_{42.7}$ alloy and its components, Ni and Co, for the HER in 1.0 mol L^{-1} NaOH solution was studied using linear polarization and impedance spectroscopy techniques.

The quasy-potentiostatic cathodic polarization curves were recorded with the scan rate of 1 mV s^{-1} in the potential range between the hydrogen reversible potential (−1.026 V) and −1.476 V, *i.e.* over the overpotential region of 0.45 V. As a measure of catalytic efficiency, the Tafel slope, b_c, and the exchange current density, j_o, were derived from the current density, j, against HER overpotential, η, plot. Data fitting was performed using the least-squares regression analysis of experimental j against η data, based on the relation:

$$j = j_0 \exp(\alpha \eta F / RT) = j_0 \exp(\eta / b_c) \quad (11)$$

where α is the charge transfer coefficient (the value used was 0.5), F is the Faraday constant, R is the gas constant, T is the absolute temperature and b_c is the cathodic Tafel slope.[7,9,13]

Figure 4 presents a comparison between the experimental and calculated Tafel plots after correction for the uncompensated IR drop has been made (the electrolyte resistance of 1.35 Ω was determined from EIS data). The symbols stand for experimental data, while the lines represent the calculated data according to [Eq. 11] The current densities were given with respect to the geometrical surface area of the electrodes. The values of the main kinetic parameters for hydrogen evolution, *i.e.* the apparent exchange current density and the Tafel slope are presented in Table 1.
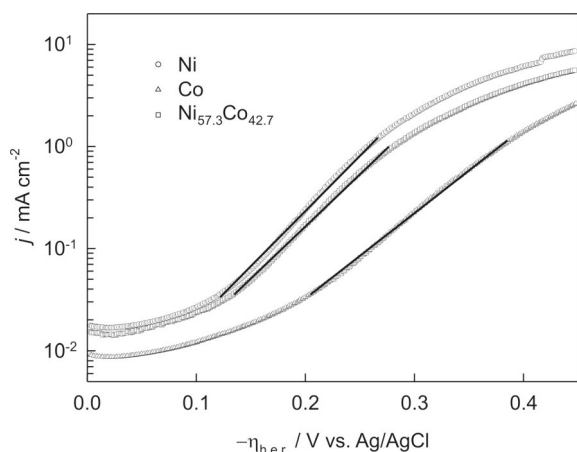
Figure 4. Quasi-potentiostatic polarization curves for Ni, Co and Ni$_{57.3}$Co$_{42.7}$ alloy in 1.0 mol L^{-1} NaOH solution, v = 1 mV s^{-1}. The symbols represent experimental data, while lines represent calculated data.

For all three investigated electrodes the Tafel slope is close to the theoretical one for the Volmer-Heyrovsky mechanism (the value equal to 118 mV dec^{-1} at 298 K). It could be noticed that the measured Tafel slopes deviate from the theoretical straight line at higher (above −0.3 V) and lower (below −0.1 V) overvoltages. The deviation of Tafel slope at higher overvoltages is probably due to the formation of hydrides in the surface layer,[11] while that at smaller overvoltages has been usually attributed to the presence of oxide film on the electrode surface.[27,28]

The obtained values for j_o, see Table 1, is reasonable to compare with literature data for polycrystalline Ni and Co under the same experimental conditions. Thus j_o of 1.7×10^{-6} A cm^{-2} obtained for polycrystalline Ni is in a good accordance with the values of j_o equal to of 1.1×10^{-6} A cm^{-2}[29] and 1.8×10^{-6} A cm^{-2}[30] reported for Ni. The value for j_o equal to 5.6×10^{-7} A cm^{-2} obtained for Co is comparable with the values j_o equal to of 8.4×10^{-6} A cm^{-2}[12] and 6.8×10^{-7} A cm^{-2}[31] reported for Co. The obtained value of

Table 1. Kinetic parameters for the HER for Ni, Co and Ni$_{57.3}$Co$_{42.7}$ alloy electrodes in 1.0 mol L^{-1} NaOH solution.

	Linear polarization		EIS	
	$-b_C$ / mV dec^{-1}	j_0 / A cm^{-2}	$-b_C$ / mV dec^{-1}	j_0 / A cm^{-2}
Ni	108	1.7×10^{-6}	107	2.4×10^{-6}
Co	115	5.6×10^{-7}	110	8.1×10^{-7}
Ni$_{57.3}$Co$_{42.7}$	102	1.4×10^{-6}	122	1.8×10^{-6}

j_o for Ni-Ca alloy, 1.8×10^{-6} A cm^{-2}, is significantly higher than the value for Co, but little lower than that for polycrystalline Ni.

Impedance measurements were carried out at selected applied potentials located inside the overpotential range in which the cathodic currents were recorded. Figure 5 presents the obtained spectra in the form of Bode magnitude and phase angle plots for Ni, Co and Ni$_{57.3}$Co$_{42.7}$ alloy, respectively. For all investigated electrodes the spectra are of a similar shape and indicate one time constant, τ. At high frequencies the solution resistance, R_{el}, dominates the impedance of samples and the Bode magnitude data exhibit the slopes of zero while the phase angles approach 0°. At intermediate frequencies a linear dependence of log $|Z|$ against log f and one well-defined maximum in the θ against log f plot are characteristics of a capacitive behaviour. In the low frequency region, the clearly expressed impedance plateaus, equal to the sum of R_{el} and Faradaic resistance, R_F, enabled to determine the R_F, at each applied potential. The spectra were analyzed using the ZView software for complex non-linear last squares (CNLS) fitting. These data were modelled using a modified Randles electrical equivalent circuit (EEC), which includes the solution resistance (R_{el}) in series with Faradaic resistance (R_F) of the HER, which is in parallel connection with the constant phase element (CPE) in a place of capacitance. The same EEC was used to model EIS data obtained on bulk Ni in alkaline solutions by several research groups.[8,30,32,33]
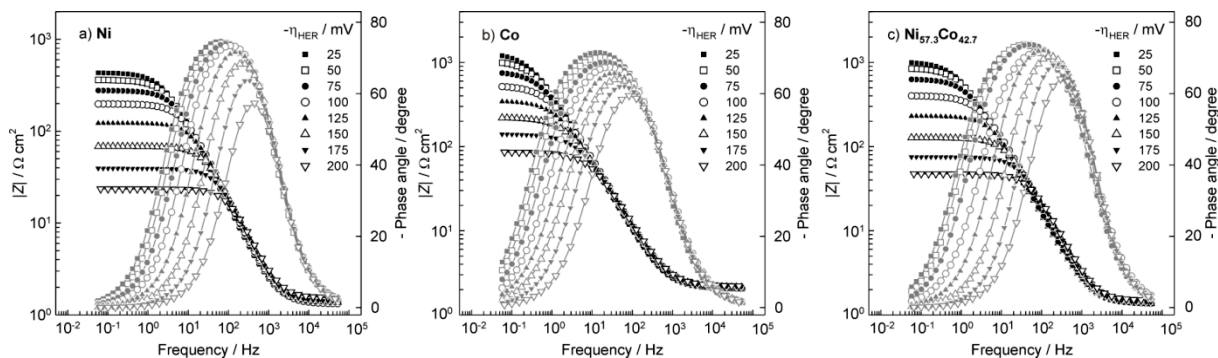

Figure 5. Impedance spectra (Bode plots) recorded on Ni (a), Co (b) and Ni-Co alloy (c) in 1.0 mol L^{-1} NaOH solution at various overpotentials.

The impedance of the CPE element is given by Z(CPE) = $[Q\,(j\omega)^n]^{-1}$, where ω is the angular frequency, n is the CPE power,[34] and Q is the frequency independent constant, which is used to calculate the interfacial capacitance (C), i.e., the double layer capacitance (C_{dl}) according to the Brug's relation:[7,35]

$$C = Q^{\frac{1}{n}}\left[R_{el}^{-1} + R^{-1} \right]^{\frac{n-1}{n}} \tag{12}$$

The electrode capacitance and the Faradaic resistance values are presented as a function of the applied potential in Figures 6 and 7, respectively.

The electrode capacitance derived from the impedance response for each electrode consists of the double layer capacitance and the pseudocapacitance, C_θ, i.e. $C = C_{dl} + C_\theta$. The pseudocapacitance is associated with potential dependence of the surface density of states of adsorbed intermediate generated in the course of the HER[11,12,36,37], and can be defined as $q \times (\partial\theta / \partial E)$, where q is the charge required to form the monolayer of adsorbed hydrogen intermediate in the overall faradaic reaction, θ is the surface coverage fraction, and E is the applied potential. The value of C_θ contributes significantly to the electrode capacitance only at low overpotentials, and it decreases rapidly to zero as the overpotential increases. Thus, the lowest C value reached at higher overpotentials, equal to 61 µF cm^{-2} for Ni, 89 µF cm^{-2} for Co, and 48 µF cm^{-2} for Ni$_{57.3}$Co$_{42.7}$ alloy (Figure 6), corresponds to the double-layer capacitance. Assuming that the double-layer of a smooth metal surface is equal to 20 µF cm^{-2},[11,38,39] the surface roughness factors of the electrodes were estimated to be $r = 3.1$ for Ni, $r = 4.4$ for Co, and $r = 2.4$ for NiCo. The value of r enables to determine the exchange current density value for a real electrode surface.
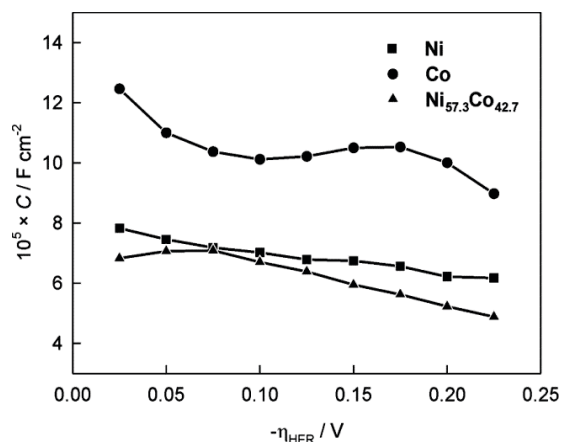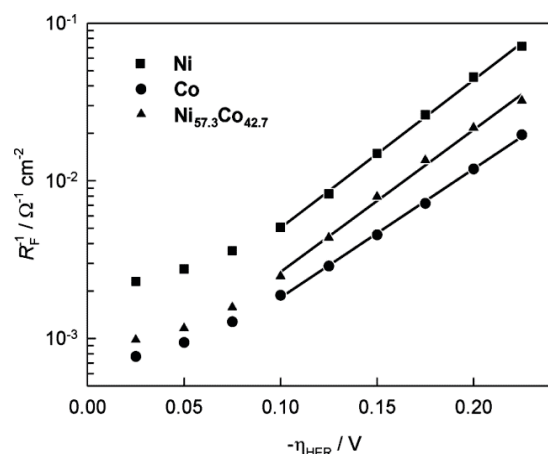
The total Faradaic resistance of the working electrode, R_F, and its reciprocal is directly related to the HER current density at the corresponding overpotential. For all investigated catalysts a linear relationship $-\eta$ versus log R_F^{-1} is observed (see Figure 7). The exchange current densities, j_0, which represents the magnitude of the rate of H$_2$ evolution, were derived from the intercepts of these lines at zero overpotential according to [Eq. (13)]:[9,13]

$$\left(\frac{\partial\eta}{\partial j} \right)_{\eta \to 0} = \frac{RT}{nF}\frac{1}{j_0} = \frac{1}{R_F} \tag{13}$$

The log R_F^{-1} against $-\eta$ dependence presented in Figure 7 is linear inside the overvoltage region between −0.1 V and −0.2 V for all investigated catalysts. The slope of these straight lines represents the Tafel slopes b_c, which numerical values are presented in Table 1. Extrapolating the linear R_F^{-1} against η straight line to the HER zero overpotential (−1.026 V) yields the apparent exchange current density, which is now possible to correct with regard to the known surfaces roughness. Thus, the exchange current densities, derived from the EIS measurements, related to the real electrode surface is presented in Table 1. The obtained value for Ni$_{57.3}$Co$_{42.7}$ alloy is slightly lower than that for polycrystalline Ni but is greater than that for polycrystalline Co. Obtained values for cathodic Tafel slopes b_c and exchange current densities are in good accordance with the values obtained from quasi-potentiostatic dc measurements. Lupi et al.[31] have shown that the highest exchange current densities were measured for the Ni-Co alloys with the Co content between 41 and 64 weight percent. It means that the synergism of the catalytic properties of nickel (low hydrogen over-potential) and of

Figure 6. The dependence of the electrode capacity C on the HER overpotential, η, in 1.0 mol L^{-1} NaOH solution.

Figure 7. The reciprocal Faraday resistance (1 / R_F) against η relationships for the HER on Ni, Co and Ni$_{57.3}$Co$_{42.7}$ alloy in 1.0 mol L^{-1} NaOH solution.

cobalt (high hydrogen adsorption) is best realized at these electrodes. Investigated $Ni_{57.3}Co_{42.7}$ alloy is at the lower limit of recommended Co concentration interval. The alloy with higher concentration of Co might have probably the better catalytic activity toward the HER.

CONCLUSIONS

The cyclic voltammetry measurements with polycrystalline Ni, Co and $Ni_{57.3}Co_{42.7}$ alloy electrodes performed in a wide potential range, from hydrogen to oxygen evolution, clearly show the potential range of formation and reduction of metal oxides / hydroxides. The obtained current maxima in voltamograms are clearly identified using literature data for reversible potentials.

The electrocatalytic efficiency of $Ni_{57.3}Co_{42.7}$ alloy was investigated by means of quasy-potentiostatic linear polarization and electrochemical impedance spectroscopy for hydrogen evolution reaction and compared with efficiency of Ni and Co derived under the same conditions. The kinetic parameters, the exchange current densities, j_0, and Tafel slopes, b_c, indicative for the HER activity for all electrodes, were determined.

Electrochemical impedance data were fitted using modified Randles electrical equivalent circuit (EEC). Electrode capacity, C, was calculated using the Brug's equation. From the values for double layer capacity at high HER overpotentials the surface roughness of the electrodes was derived.

The impedance results agree well with the results obtained from quasy-potentiostatic linear polarization measurements. Obtained cathodic Tafel slopes for all investigated electrodes are close 118 mV dec^{-1}, confirming that the main pathway for the HER at investigated electrode materials is Volmer-Heyrovski with Heyrovsky as the rate determining step.

Electrocatalytic activity of the $Ni_{57.3}Co_{42.7}$ alloy is higher than that of Co electrode, but lower than that of Ni electrode. The true intrinsic activity of the alloy probably can be improved with increasing the cobalt content.

REFERENCES

[1] L. Valek, M. Metikoš-Huković, Z. Grubač, *J. New. Mat. Electrochem. Systems* **2006**, *9,* 145.

[2] C. Lupi, A. Dell'Era, M. Pasquali, *Int. J. Hydrogen Energy* **2014**, *39*, 1932.

[3] J. M. Jakšić, M. V. Vojnović, N. V. Krstajić, *Electrochim. Acta* **2000**, *45*, 4151.

[4] M. A, Dominegz-Crespo, M. Plata-Tores, A. M. Torres-Huerta, E. M. Arce-Estrada, J. M. Hallen-Lopet, *Materials Characterization* **2005**, *55*, 83.

[5] S. Voskanyan, G. Pchelarov, R. Rashkov, K. Petrov, *Bulg. Chem. Commun.* **2016**, *48*, 78.

[6] C. Gonzalez-Buch, I. Herraiz-Cardona, E. Ortega, J. Garcia-Anton, V. Perez-Herranz, *Int. J. Hydrogen Energy* **2013,** *38*, 10157.

[7] Z. Grubač, M. Metikoš-Huković, R. Babić, *Int. J. Hydrogen Energy* **2013**, *38*, 4437.

[8] Ž. Petrović, M. Metikoš-Huković, Z. Grubač, S. Omanović, *Thin Solid Films*. **2006**, *513*; 193.

[9] M. Metikoš-Huković, Z. Grubač, N. Radić, P. Dubček, I. Djerdj, *Electrochem. Commun.* **2007**, *9,* 299.

[10] S. Martinez, M. Metikoš-Huković, L. Valek, *Mol. Catal. A: Chem.* **2005**, *245*, 114.

[11] M. Metikoš-Huković, A. Jukić, *Electrochim. Acta* **2000** , *45,* 4159.

[12] A. Jukić, J. Piljac, M. Metikoš-Huković, *J. Mol. Catal. A: Chem.* **2001**, *166*, 293.

[13] M. Metikoš-Huković, Z. Grubač, N. Radić, A. Tonejc, *Mol. Catal. A: Chem.* **2006**, *249*, 172.

[14] Z. Grubač, Ž. Petrović, J. Katić, M. Metikoš-Huković, R. Babić, *J. Electroanal. Chem.* **2010**, *645*, 87.

[15] M. Behazin, M.C. Biesinger, J. J. Noël, J. C. Wren, *Corros. Sci.* **2012**, *63*, 40.

[16] A. Jukić, M. Metikoš-Huković*, Electrochim. Acta* **2003**, *48*, 3929.

[17] C.V. D'Alkaine, M.A. Santanna, *J. Electroanal. Chem*. **1998**, *457*, 5.

[18] W. Visscher, E. Barendrecht, *Electrochim. Acta* **1980**, *25*, 651.

[19] J. L. Ord, *Surface Sci.* **1976**, *56*, 413.

[20] N. Sato, K. Kudo, *Electrochim. Acta* **1974**, *19*, 461.

[21] K. M. Ismail, W. A. Badawy, *J. Appl. Electrochem*. **2000**, *30*, 1303.

[22] L. D. Burke, M. E. Lyons, O. J. Murphy, *J. Electroanal. Chem*. **1982**, *132*, 247.

[23] H. Gomez Meier, J. R. Vilche, A. J. Arvia, *J. Electroanal. Chem.* **1982**, *134,* 251.

[24] W. K. Behl, J.E. Toni, *J. Electroanal. Chem*. **1971**, *31,* 63.

[25] N. Sato, T. Ohtsuka, *J. Electrochem. Soc*. **1978**, *125*, 1735.

[26] M. Pourbaix, *Atlas of Electrochemical Equilibria in Aqueous Solutions,* NACE International, 2nd Ed., **1976**.

[27] B. Losiewicz, A. Budniok, E. Rowinski, E. Lagiewka, A. Lasia, *Int. J. Hydrogen Energy* **2004**, 29145.

[28] A. Krolikowski, A. Wiecko, *Electrochim. Acta* **2002**, *47*, 2065.

[29] N. Krstajić, M. Popović, B. Grgur, M. Vojnović, D. Šerpa, *J. Electroanal. Chem.* **2001**, *512* 16.

[30] A. Lasia, A. Rami, *J. Electroanal. Chem.* **1990**, *294*, 123.

DOI: 10.5562/cca3174

Croat. Chem. Acta **2017**, *90*(*2*), 273–280

[31] C. Lupi, A. Dell'Era, M. Pasquali, *Int. J. Hydrogen Energy* **2009**, *34*, 2101.

[32] P. Elumalai, H.N. Vasan, N. Munichandraiah, S. A. Shivashankar, *J. Appl. Electrochem*. **2002,** *32*, 1005.

[33] Y. Petrov, J.-P. Schosger, Z. Stoynov, F. de Bruijn, *Int. J. Hydrogen Energy* **2011**, *36*, 12715.

[34] J. Jorcin, M. E. Orazem, N. Pébére, B. Tribollet, *Electrochim. Acta* **2006**, *51*, 1473.

[35] G. J. Brug, A. L. G. van der Eeden, M. Sluyters-Rehbach, J. H. Sluyters, *J. Electroanal. Chem.* **1984**, *176*, 275.

[36] T. Liu, B. E. Conway, *J. Appl. Electrochem*. **1987**, 17, 983.

[37] B. V. Tilak, B. E. Conway, *Electrochim. Acta* **1976**, *21*, 745.

[38] L. Chen, A. Lasia, *J. Electrochem. Soc*. **1992**, *139*, 3214.

[39] R. K. Shervedani, A. Lasia, *J. Appl. Electrochem*. **1999**, *29*, 979.